Study of Free Surface Flows in Rectangular Channel over Rough Beds

S. H. Talbi[1], A. Soualmia[1†], L. Cassan[2] and L. Masbernat[2]

[1] *National Institute of Agronomy of Tunisia (Laboratory of Water Sciences and Technology), El Manzeh, Tunis, 1002, Tunisia*
[2] *Institute of Fluid Mechanics of Toulouse, INP Toulouse, 31400, France*

†*Corresponding Author Email: amel.inat@hotmail.fr*

ABSTRACT

This paper presents the results of an experimental and numerical study of fully developed flow in a straight rectangular open channel over rough beds. Conical ribs were placed on the flume bottom to simulate different bed roughness conditions. Acoustic Doppler Velocimetry (ADV) measurements were made to obtain the velocity components profiles as well as the Reynolds stress profiles, at various locations. The experimental results are validated by simulations using an algebraic stress model. These investigations could be useful for researches in the field of sediment transport, bank protection, etc.

NOMENCLATURE

$C(K_S^+)$	roughness function	x	longitudinal coordinate
k	turbulent kinetic energy	y	transverse coordinate
K_S	roughness height	z	vertical coordinate
K_S^+	roughness number		
U	longitudinal mean velocity	α	bed slope
u, v, w	turbulent fluctuations	ε	dissipation rate of k
u_*	friction velocity	κ	Von Karman constant
V	transverse mean velocity	λ	length of symmetrical cell
W	vertical mean velocity	Ω	vorticity of secondary flows
		ψ	stream function

1. INTRODUCTION

The study of turbulent flow over rough surfaces is considered highly important in hydraulic engineering and is an active area of research, because practically all surfaces in open-channel flow can be considered rough (Bomminayuni *et al.* 2011). And prediction of roughness effects is of clear practical importance for a wide range of industrial and geophysical flows. Also, turbulent free surface flows present complex distribution of the bed shear stress that can undulate in the transverse direction, due to the roughness variations of fixed or mobile beds (Soualmia *et al.* 2010).

Experimental study of these processes requires flow-measuring devices with adequate spatial and temporal resolution (Voulgaris *et al.* 1998). At the beginning, extensive experimental research has been undertaken on the mean and turbulence characteristics of open channel flow with the aid of the hot film anemometers (Blinco *et al.* 1971; Nakagawa *et al.* 1981). In addition, the introduction of the Acoustic Doppler Velocimetry (ADV) provided another tool for nonintrusive measurements of turbulent flow in the laboratory.

In fact the development of the acoustic sensors offered measurements of the instantaneous three-dimensional flow components at high sampling rates (Song *et al.* 2001). The sensors require no calibration and have low noise levels, but their large sample volume limits the resolution of turbulence eddy scales and the proximity to the boundary.

In the present work, the ability of the ADV sensor to measure turbulence is examined by comparing measured turbulence parameters to the numerical results of the 3D simulations.

2. MEAN MOMENTUM BALANCE FOR FULLY DEVELOPED FLOWS

Fully developed flows are considered in straight rectangular open channels with constant bed slope α. Let (x, y, z) be an orthogonal coordinate system in which x and y are the longitudinal and transverse coordinates, and the z-axis is normal to the channel bottom. The components of the mean velocity and the turbulent fluctuations in the x, y and z coordinate directions are denoted by U, V, W and u, v, w, respectively.

The flow being fully developed in the x-direction, all the mean quantities are only dependent on y and z coordinates and we can express the equations for the mean motion in terms of the quantities (U, Ψ, Ω), in which Ψ and Ω are the stream function and the vorticity of secondary flows, respectively. Neglecting the effect of the viscosity, the equations of U, Ψ, Ω (the 3D model) can be wrote as:

$$\frac{\partial VU}{\partial y} + \frac{\partial WU}{\partial z} = \frac{\partial}{\partial z}(-\overline{uw}) + \frac{\partial}{\partial y}(-\overline{uv}) + g\sin\alpha \quad (1)$$

$$\frac{\partial V\Omega}{\partial y} + \frac{\partial W\Omega}{\partial z} = -\frac{\partial^2}{\partial y\partial z}(\overline{w^2} - \overline{v^2}) + (\frac{\partial^2}{\partial z^2} - \frac{\partial^2}{\partial y^2})(-\overline{vw}) \quad (2)$$

$$\nabla^2\psi = -\Omega, \quad V = \frac{\partial\psi}{\partial z}, \quad W = -\frac{\partial\psi}{\partial y} \quad (3)$$

The prediction of the mean velocity field from Eq. (1) to Eq. (3), requires second-order closure models of the Reynolds stresses notably allowing an accurate calculation of the turbulence anisotropy term $\partial^2(\overline{w^2} - \overline{v^2})/\partial y\partial z$ that plays a main role in the generation of the secondary flow vorticity (Eq. (2)).

3. NUMERICAL FRAMEWORK

3.1 Algebraic Reynolds Stress Model

In the 3D model (Eq. (1), Eq. (2) and Eq. (3)), the turbulent stresses were expressed by a model issued from the Reynolds stress transport model of Gibson and Rodi, including surface proximity functions to simulate the effects of the wall and the free surface on the turbulence anisotropy. In fact the components of the Reynolds tensor present in Eqs. (1) and (2) were written as (Gibson and Rodi. 1989):

$$-\overline{uv} = C_{\mu y}\frac{k^2}{\varepsilon}\frac{\partial U}{\partial y} \quad ; \quad -\overline{uw} = C_{\mu z}\frac{k^2}{\varepsilon}\frac{\partial U}{\partial z}$$

$$and \quad -\overline{vw} = C_{\mu 0}\frac{k^2}{\varepsilon}\left(\frac{\partial V}{\partial z} + \frac{\partial W}{\partial y}\right) \quad (4)$$

$$C_{\mu y} = \frac{1-C_2}{C_1 + \hat{P} - 1}\frac{\overline{v^2}}{k} ; C_{\mu z} = \frac{1-C_2 + \frac{3}{2}C_2 c_2' f}{C_1 + \hat{P} - 1 + \frac{3}{2}c_1' f}\frac{\overline{w^2}}{k} \quad (5)$$

$$(C_1 + \hat{P} - 1)\frac{\overline{v^2}}{k} = \frac{3}{2}(C_1 - 1) + \frac{3}{2}C_2\hat{P}(1 + c_2' f) + c_1'\frac{\overline{w^2}}{k}f + G_{v,ES} \quad (6a)$$

$$G_{v,ES} = 2(1-C_2)(-\frac{\overline{v^2}}{\varepsilon}\frac{\partial V}{\partial y} - \frac{\overline{vw}}{\varepsilon}\frac{\partial V}{\partial z}) - 2c_2'C_2 f(-\frac{\overline{w^2}}{\varepsilon}\frac{\partial W}{\partial z} - \frac{\overline{vw}}{\varepsilon}\frac{\partial W}{\partial y}) \quad (6b)$$

$$(C_1 + \hat{P} - 1 + 2c_1' f)\frac{\overline{w^2}}{k} = \frac{3}{2}(C_1 - 1) + \frac{3}{2}C_2\hat{P}(1 - 2c_2' f) + G_{w,ES} \quad (7a)$$

$$G_{w,ES} = 2(1 - C_2 + 2C_2 c_2' f)(-\frac{\overline{vw}}{\varepsilon}\frac{\partial W}{\partial y} - \frac{\overline{w^2}}{\varepsilon}\frac{\partial W}{\partial z}) \quad (7b)$$

$\hat{P} = P/\varepsilon$ is the ratio between the turbulent kinetic energy and its dissipation rate ε ; C_1, C_2, c'_1 and c'_2 are constants. In Eqs. (6) to (7), the surface proximity function f= $f_b + f_s$ only contains the contributions f_b of the bottom and f_s of the free surface to the turbulence anisotropy increase ; in the test cases considered here there are not lateral walls. For the functions f_b and f_s, the expressions proposed by Gibson and Rodi were adopted: f=$f_b + f_s$, with

$$f_b = \frac{L(1-\xi)^2}{ah\xi} \quad ; \quad f_s = \frac{L\xi^2}{ah(1-\xi)} \quad (8)$$

$$V\frac{\partial k}{\partial y} + W\frac{\partial k}{\partial z} = \frac{\partial}{\partial y}(c_k\frac{\overline{v^2}}{k}\frac{k^2}{\varepsilon}\frac{\partial k}{\partial y}) + \frac{\partial}{\partial z}(c_k\frac{\overline{w^2}}{k}\frac{k^2}{\varepsilon}\frac{\partial k}{\partial z}) + P - \varepsilon \quad (9)$$

$$V\frac{\partial\varepsilon}{\partial y} + W\frac{\partial\varepsilon}{\partial z} = \frac{\partial}{\partial y}(c_\varepsilon\frac{\overline{v^2}}{k}\frac{k^2}{\varepsilon}\frac{\partial\varepsilon}{\partial y}) + \frac{\partial}{\partial z}(c_\varepsilon\frac{\overline{w^2}}{k}\frac{k^2}{\varepsilon}\frac{\partial\varepsilon}{\partial z})$$

$$+ 0.47\frac{k}{\varepsilon} + 3.9\frac{\varepsilon^2}{k}\frac{b_{ij}b_{ij}}{1 + 1.5\sqrt{b_{ij}b_{ij}}} - C_{\varepsilon 2}\frac{\varepsilon^2}{k} \quad (10)$$

In which $b_{ij} = ((\overline{u_i u_j} - (2/3)k\delta_{ij})/2k)$ is the anisotropy tensor. L is the energy containing eddy length scale, defined as L=$k^{3/2}/\varepsilon$; h is the water depth, ξ=z/h and a is a constant. The transport equation of the turbulent kinetic energy and the dissipation rate complete the Reynolds stress model. The model constants are listed in Table 1:

Table 1 Constants of the model

C_1	C_2	c_1'	C_2'	a	$C_{\varepsilon 1}$	$C_{\varepsilon 2}$	c_k	c_ε
1.8	0.6	0.5	0.3	3.18	1.44	1.92	0.22	0.18

The numerical method employed to solve the system of partial differential equation uses a finite volume method, and the resolution is iteratively by stone method. Because of symmetrical conditions the resolution is considered only on the half cross section of the channel. A mesh of 70 x 25 grids (leading to square cells) uniformly distributed is used. Test calculations were also carried out with coarser grids, these yielded to secondary velocities which differed by less than 2% from the obtained with the actual grids.

3.2 Boundary Conditions

At the wall, z=0 and 0≤y≤ λ: The longitudinal mean velocity is given by the logarithmic law:

$$\frac{U}{u_*} = \frac{1}{\kappa}\ln(u_*\frac{(z+z_0)}{\nu}) + C(K_S^+) \quad (11)$$

In which u_* is the local friction velocity, z_0 the shift of the origin of the logarithmic law and C (K_S^+) a function of the roughness number $K_S^+ = (u_* K_S)/\nu$ in

which K_S is a roughness height. In the applications of the model, the transverse distribution of $C(K_S^+)$ and z_0 are determined from experiments. The wall boundary conditions for k and ε express the equilibrium between production and dissipation, as:

$$k=C_\mu^{-0.5}u_*^2 \quad , \quad \varepsilon=u_*^3/(\kappa(z+z_0)) \qquad (12)$$

At the free surface and on the lateral boundaries, symmetry conditions were imposed.

$$\frac{\partial U}{\partial y} = \frac{\partial k}{\partial y} = 0 \qquad (13)$$

The boundary conditions for the secondary flow are expressed in terms of the stream function Ψ and the longitudinal vorticity Ω taken as Ψ = 0 and Ω = 0 on the limits of the integration cross-section.

4. EXPERIMENTAL SETUP

All homogeneous and inhomogeneous rough bottom experiments reported in this study were conducted in a straight rectangular tilting flume that was 8m long, 1m wide and 0.5m deep (Fig. 1). The settling tank was located at the entrance to the flume and equipped with turbulence reduction screens. At the end of the channel, water was collected through a tank and recirculated with a pump. The discharge was measured with an ultrasound flow meter installed on the supply pipe.

Fig. 1. Open channel flume used in experiments (IMFT, 2015).

The depth of flow (h) was kept constant so that h=0.1m. Detailed information on the hydraulic and geometric conditions is given in Table. 2. All measurements are carried out at a streamwise location x=4.8m from the flume entrance, where the flow field is fully developed.

Nearly instantaneous profiles of three components of flow velocity and turbulence characteristics in the water column were measured by using an Acoustic Doppler Velocity (Fig. 2). Measurements were carried out at a frequency of 50Hz during 3min, which guarantees reliable estimates of the mean velocities and the Reynolds stresses.

The ADV operates on a pulse-to-pulse coherent Doppler shift to provide a three-component velocity. Acoustic waves with a frequency f_0=10MHz and a speed c are emitted by a transducer (emitter). These waves pass through a water column and arrive at the measuring point which is located about 5 cm below the transducer (Firoozabadi *et al*. 2010).

At this point they are reflected by the ambient particles within the flow. The waves reflected toward the receiver have a frequency f_r. The difference $f_d=(f_0-f_r)$ is the Doppler-shift frequency. Each receiver of the ADV measures the projection of the 3D water velocity onto its bistatic axis by detecting the Doppler-shift frequency. The data of these measurements were analyzed using the free software WinADV (Song and al. 2001).

Fig. 2. 3-D acoustic probe.

The channel bed is artificially roughened by conical ribs with a ratio of the roughness height (K_S) to the total depth of flow (h) equal to 0.08. Also, the ratio of the pitch (p) to the roughness height equal to 2. Here, p is the pitch between consecutive roughness elements. So in this work, we studied the d-type roughness ((p/K_S)<5) (Perry *et al*. 1969).

These experimental and numerical studies were applied to two different configurations of model roughness. In a first step, we studied the structure of the flow in an open channel where the bottom is completely rough (homogeneous rough bottom). In a second step, we treated the case where the bottom presents transverse gradient of roughness (inhomogeneous rough bottom).

In these experiments, the bed forms correspond to completely rough strips or to smooth strips and rough strips of characteristic height K_S, arranged in an alternate manner as indicated in (Fig. 3).

The flow depth, h, was about 10 cm resulting in a width to depth ratio (B/h) of 10. Therefore, the

channel was considered wide so that the flow in the central region of the channel was unaffected by the sidewalls, the simulations were limited to a symmetrical cell of length $\lambda = d_S + d_R$ situated in the central zone of the channel. In the 3D-simulations we adopted the function $C(K_S^+)$ of the roughness number K_S^+, which is given by the expression of Naot and Emrani (1983) to account for the transition between the rough and the smooth strips:

$$C(K_S^+) = \kappa^{-1} \ln[9K_S^+ + 20)(0.3K_S^{+2} + K_S^+ + 20)^{-1}] \quad (14)$$

a)

b)
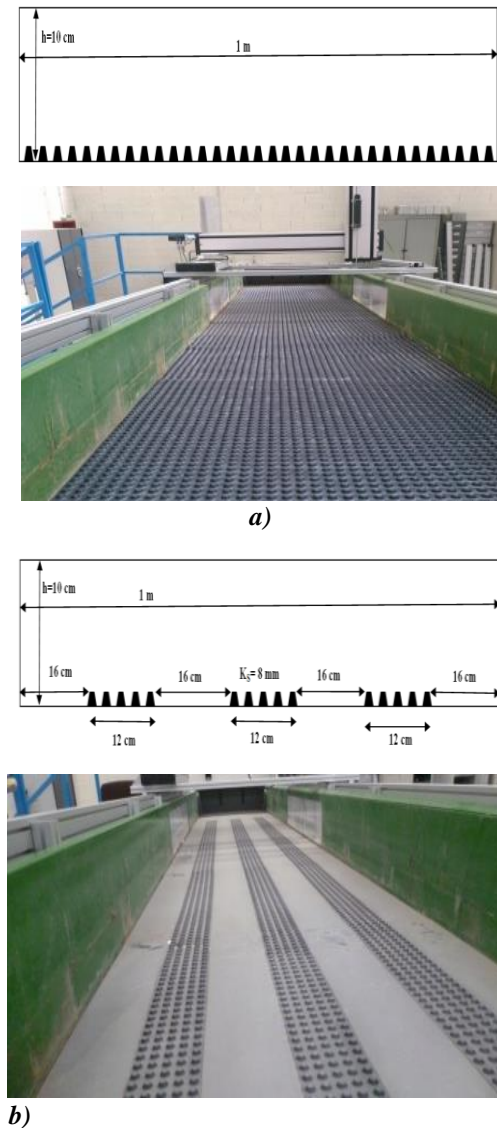
Fig. 3. Shapes of the bed forms in the different roughness configurations: a) homogeneous rough bottom and b) inhomogeneous rough bottom.

5. RESULTS AND DISCUSSION

In all the figures, the experimental results are referred by the abbreviation Exp and the results of the anisotropic model are referred by the

abbreviation NPF, (for Non Parallel Flow). On the same figures are also presented results obtained by assuming the flow is parallel (V=W=0): this case is referred by the abbreviation PF.

For our case study the acoustic probe can take measurements only in the first five centimeters close to the channel bottom. This is due to the fact that the probe measured point should be located 5 cm below the probe transducer, on other hand the acoustic probe should be entirely immersed in water.

5.1 Mean Longitudinal Velocity

In Fig. 4 we present the vertical profiles of the longitudinal velocities.

a)

b1)

b2)
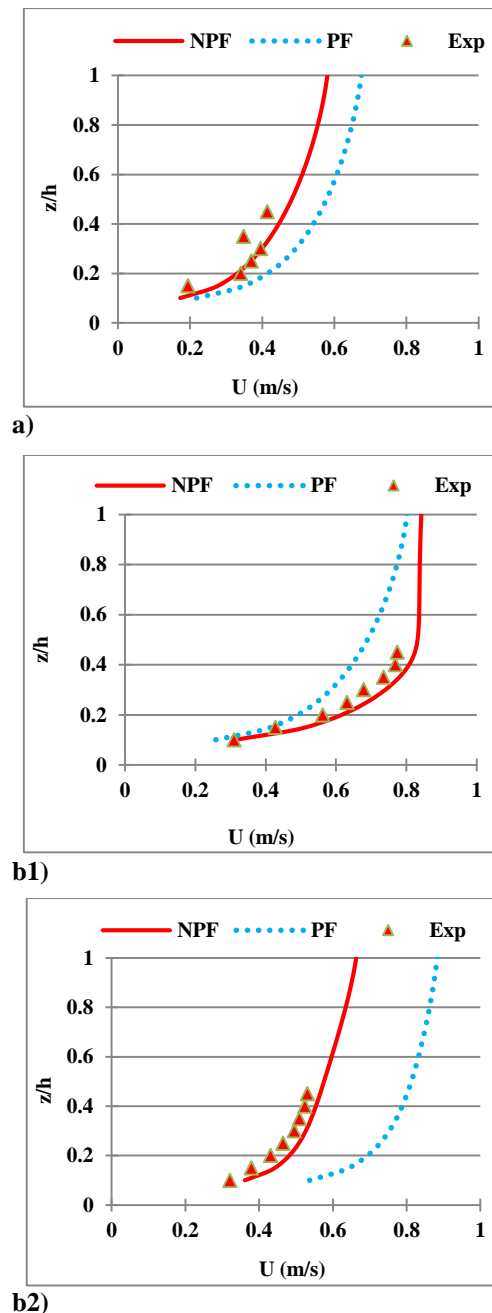
Fig. 4. Longitudinal mean velocity distribution: a) at the channel center (y/λ=0.5), b1) above the rough strips (y/λ=0.5) and b2) above the smooth strips (y/λ=1).

Table 2 Hydraulic and geometric conditions

Different configurations	Depth (h) (cm)	Discharge (Q) (l/s)	Fr (-)	Slope (α) (%)	K_S (mm)	d_S (cm)	d_R (cm)
Homogeneous rough bottom	10	43.1	0.43	0.2	8	0	100
Inhomogeneous rough bottom	10	50.8	0.51	0.2	8	16	12

Table 3 Experimental values of the friction velocity by various methods

Approaches	The friction velocity u_* (m/s)		
	Homoge-neous rough bottom	Inhomogeneous rough bottom	
		Above the rough strips	Above the smooth strips
The log law	0.03526	0.07216	0.03198
Reynolds shear stress	0.03563	0.07202	0.03407
Turbulent kinetic energy	0.03428	0.05455	0.02996
Mean friction velocity	0.03505	0.06624	0.03200

Table 4 Deviations of u_* from the mean value

Approaches	The deviations of u_* from the mean value (%)		
	Homoge-neous rough bottom	Inhomogeneous rough bottom	
		Above the rough strips	Above the smooth strips
The log law	+ 0.58	+ 8.93	- 0.07
Reynolds shear stress	+ 1.64	+ 8.72	+ 6.46
Turbulent kinetic energy	- 2.22	- 17.65	- 6.38

The experiment matches correctly with the non parallel flow (NPF) simulation above the rough strips (Fig. a) and (Fig. 4-b1) and illustrates the important effect of secondary motions. Similarly, above the smooth strips (Fig. 4-b2), the experiments results are near the non parallel flow (NPF) simulations.

5.2 Techniques for Estimating Friction Velocity

In the present work, we focus on the profile methods for the determination of the friction velocity u_*, taking advantage of the detailed quasi-instantaneous full depth ADV profiles of all three velocity components. We will evaluate the logarithmic profile method, the Reynolds stress method and in addition, apply the turbulent kinetic energy (k) method.

a) Logarithmic Velocity Profile Method

The logarithmic velocity profile method is widely used in open channel flow and river studies (Nezu and Nakagawa 1993). It has the advantage that no independent estimate of z_0 is needed, because u_* depends only on the slope of the profile, not the intercept.

The logarithmic velocity distribution is described by the Von Karman-Prandtl equation (Eq. (11)). Shear velocity is determined using velocity profile data, particularly those measured in the inner layer (Guo *et al*. 2008).

Comparison of selected measured velocity profiles and the log law is given in (Fig. 5) in which the log law is plotted as a solid line.

These results show that the measured velocity profiles agree well with the log law in the inner region.

b) Reynolds shear stress method

When turbulence measurements are available, local mean shear velocity can be determined from the measured Reynolds stress distribution in the constant stress layer where stress within the water column only varies slightly from bottom stress τ (Kim *et al*. 2000). It can be expressed as:

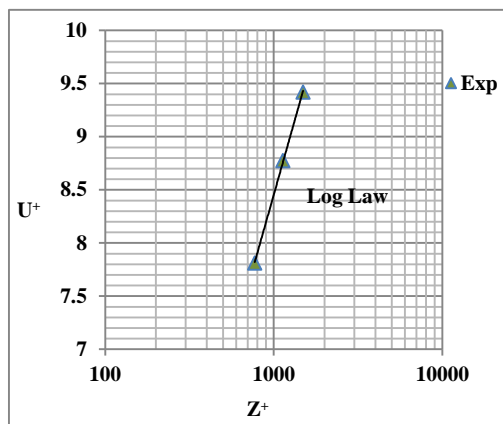$$u_*^2 = -\overline{u'w'} \tag{15}$$

Where u' and w' are the velocity fluctuations of the longitudinal and vertical components, respectively. The overbar denotes time mean values.
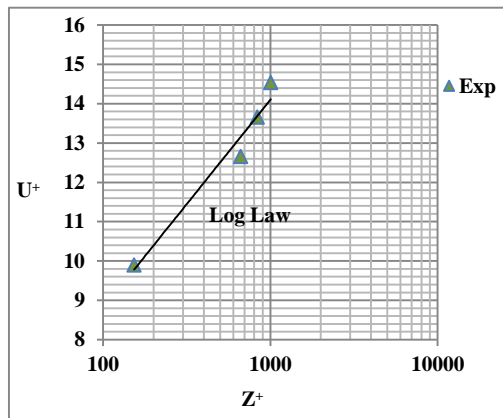
On Fig. 6 we present the vertical profiles of the Reynolds shear stress, normalized by the square of the friction velocity.
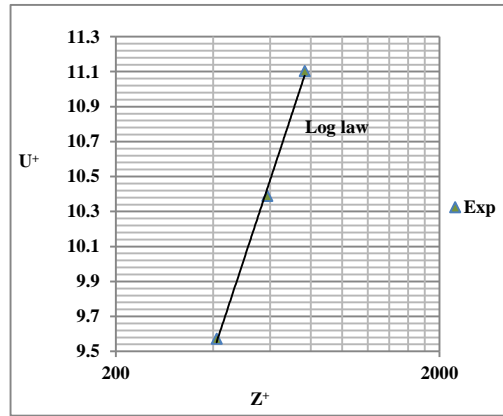
a)

b1)

b2)

Fig. 5. Comparison of measured longitudinal velocity and Log law: a) at the channel center (y/λ=0.5), b1) above the rough strips (y/λ=0.5) and b2) above the smooth strips (y/λ=1).

Figure 6 clearly shows that the measured velocity distributions fit better with the NPF simulation. So this confirms the existence of the secondary currents in turbulent flows as well as their effect on the structure of the flow.
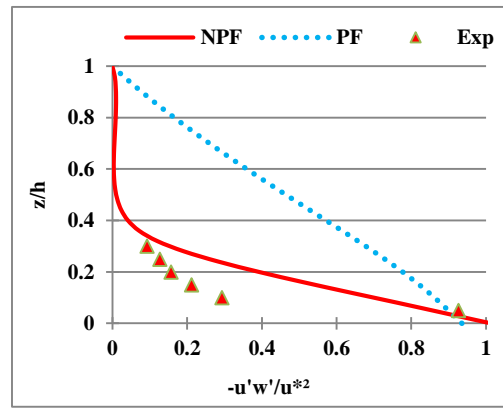
c) Turbulent Kinetic Energy Method

Bed shear stress can be obtained from turbulent

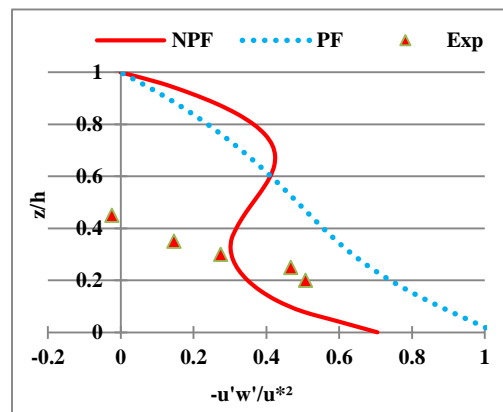velocity fluctuations through k calculations. k is defined as:

$$k = 0.5 \ (\overline{u'}^2 + \overline{v'}^2 + \overline{w'}^2) \qquad (16)$$
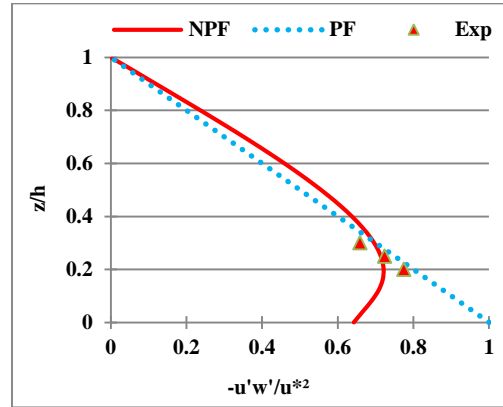
a)

b1)

b2)

Fig. 6. Vertical profiles of the turbulent shear stress: a) at the channel center (y/λ=0.5), b1) above the rough strips (y/λ=0.5) and b2) above the smooth strips(y/λ=1).

Where v' is the fluctuating transversal velocity component. Linear relationships between k and shear stress have been formulated (Townsend 1976). Soulsby (1980) found that the average ratio of shear stress to k is constant:
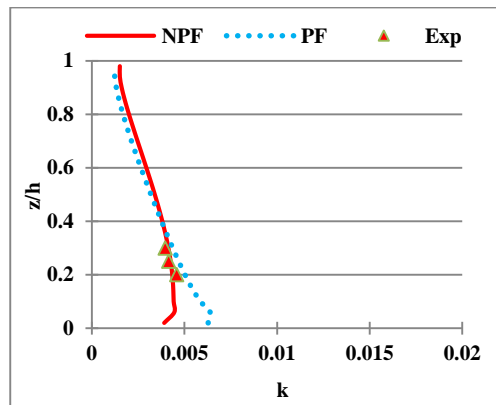
$$\tau = \beta \, \rho \, k \tag{17}$$
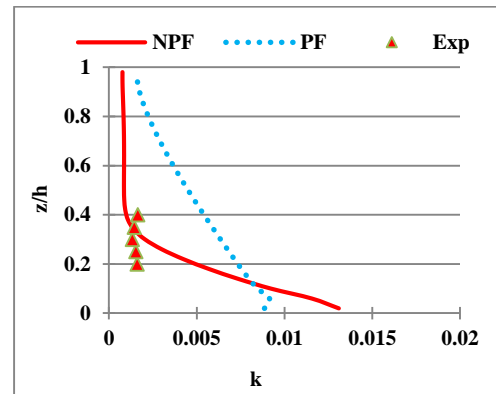
Therefore,

$$u_* = \sqrt{\beta \, k} \tag{18}$$

Where β is proportionality constant. For oceanic conditions, Soulsby (1980) suggested β=0.2 while Stapleton and Huntley (1995) applied β=0.19 which is also used for atmospheric boundary layers.
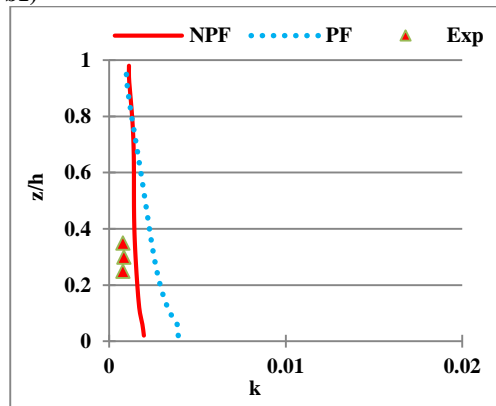
So, we obtain:

$$u_* = \sqrt{0.2 \, k} \quad When \quad z \rightarrow 0 \tag{19}$$

a)

b1)

b2)

Fig. 7. Vertical profiles of the turbulent kinetic energy: a) at the channel center (y/λ=0.5), b1) above the rough strips (y/λ=0.5) and b2) above the smooth strips(y/λ=1).

So to determine the experimental values of the friction velocity we used three methods. Firstly, u_* is estimated by fitting a logarithmic profile to the measured velocities, secondly, we used the profiles of the Reynolds shear stress -u'w'. Finally, we tested the turbulent kinetic energy. The friction velocity values obtained using the different methods for all the experiments are summarized as follow in the Table 3.

The experimental values obtained by these three methods are generally acceptable and are very close to the average value. So, results from all methods fall into a range of -17.31% and +9.17% variability from the mean value.

The estimates obtained from the log law and the Reynolds shear stress methods reasonably agree, while the results deduced from the turbulent kinetic energy method are within 17.31% of the mean value over inhomogeneous rough bottom.

The friction velocities deviations from the mean value are shown in the following table.

The average value of the experimentally friction velocity determined from these three methods are presented in Fig. 8.
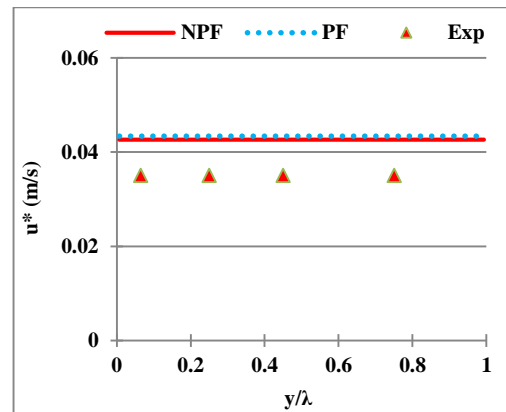

a)
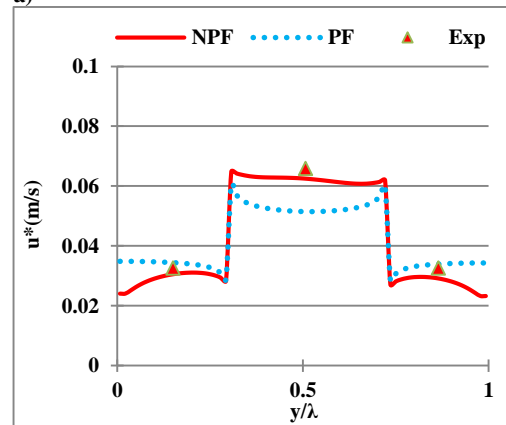
b)

Fig. 8. Transverse distribution of the friction velocity: a) homogeneous rough bottom and b) inhomogeneous rough bottom.

In the case where the bottom is completely rough and with applying the symmetry condition (wide

channel), the friction velocity remains constant throughout the channel bandwidth (λ). On the other hand over inhomogeneous rough bottom (Fig. 8 (b)) we observed the effect of the sharp roughness change on the distribution of u_*, and a good agreement with experimental results. The differences between NPF and PF simulations underline the effects of secondary flows that increase the bottom friction above the rough strips and decrease it above the smooth strips.

Figures 9 and 10 show calculated (a) and measured (b) secondary currents in the considered part of the channel cross section.

a)

b)

Fig. 9. Secondary currents velocity vector over homogeneous rough bottom: a) Simulation b) Experiment.
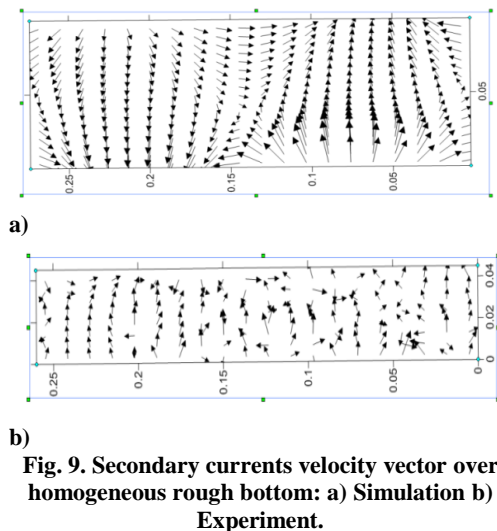
Over the homogeneous rough bottom, some deviations from measurements are found in the location of the vortex core and in the size of the vortices.

a)

b)

Fig. 10. Secondary currents velocity vector over inhomogeneous rough bottom: a) Simulation b) Experiment.
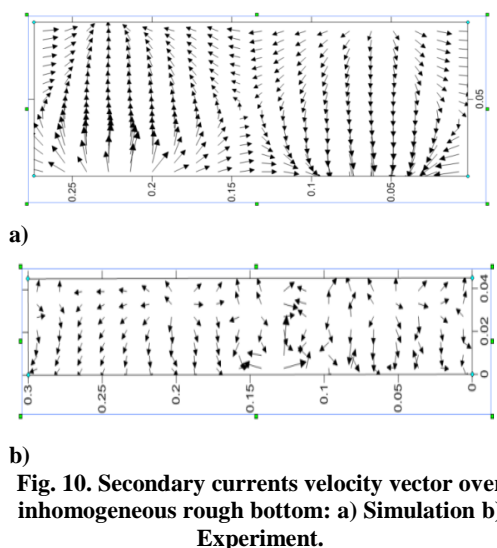
Over the non-homogeneous rough bottom, the numerical simulations reported on Fig. 10-a confirmed the experiments: well reproduction of the cellular organization of the secondary flows, which are oriented from the rough zone towards the smooth one. Also, the downward movement of the fluid over the rough strips and the upward movement over the

smooth strips is matched quite accurately.

5. CONCLUSION

In this study, measurements of the mean and turbulence characteristics in open channel flows over rough beds were carried out using a 3D Acoustic Doppler Velocimetry. Firstly, experimental measurements have been carried out from homogeneous and inhomogeneous rough bottom to document the turbulence structure in the vicinity of the bottom wall. Secondly, 3D-simulations were achieved using an anisotropic algebraic Reynolds stress model to check the experiments. A relatively good agreement between measurements and the 3D calculations was obtained. So, the reported experiments can constitute benchmark test cases allowing the improvement and validation of numerical models.

REFERENCES

Bagherimiyab, F. and U. Lemmin (2013). Shear velocity estimates in rough bed open channel flow. *Earth surface processes and landforms* 38, 1714-1724.

Bomminayuni, S. and T. Stoesser (2011). Turbulence statistics in an open-channel flow over a rough bed. *Journal of Hydraulic Engineering 137*(1), 1347-1358.

Bonakdari, H., F. Larrarte and L. Lassabatere (2008). Turbulent velocity profile in fully-developed open channel flows.

Chen, X. and Y. M. Chiew (2003). Response of velocity and turbulence to sudden change of bed roughness in open-channel flow. *Journal of Hydraulic Engineering* 129(1), 35-43.

Firoozabadi, B., H. Afshin and A. Bagherpour (2010). Experimental investigation of turbulence specifications of turbidity currents. *Journal of Applied Fluid Mechanics 3*(1), 63-73.

Florens, E., O. Eiff and F. Y. Moulin (2013). Defining the roughness sublayer and its turbulence statistics. *Experiments in fluids* 54(4), 1-15.

Gibson, M. M. and W. Rodi (1989). Simulation of free surface effects on turbulence with a Reynolds stress model. *Journal of Hydraulic Research* 27(1), 233-245.

Guo, J. and P. Y. Julien (2008). Application of the modified log-wake law in open channels.

Journal of Applied Fluid Mechanics 1(2), 17-23.

Jimenez, J. (2004). Turbulent flow over rough walls. *Annual Reviews Journal of Fluid Mechanics 36*, 173-196.

Kim, S. C., C. T. Friedrichs, J. P. Y. Maa and L. D. Wright (2000). Estimating bottom stress in a tidal boundary layer from acoustic doppler velocimeter data. *Journal of Hydraulic Engineering 126*, 399-406.

Knight, D. W (1981). Boundary shear in smooth and rough channels. *Journal of Hydraulic Engineering, Hydrologic Science Division 107*(7), 839-851.

Knight, D. W., J. D. Demetriou and M. E. Hamed (1984). Boundary shear in smooth rectangular channels. *Journal of Hydraulic Engineering, Hydrologic Science Division 110*(4), 405-422.

Labiod, C. (2005). *Etude des écoulements à surface libre sur fond rugueux*. Ph. D. thesis, Institute of Fluid Mechanics of Toulouse, Toulouse, France.

Muller, A. and X. Studerus (1979). Secondary flows in open channel. In *Proceedings Congress of the International Associations for Hydraulic Research, Italy* 19-24.

Naot, D. and S. Emrani (1983). Numerical simulation of the hydrodynamic behavior of fuel rod with longitudinal cooling fins. *Nuclear Engrs. and Des 73*, 319-329.

Nezu, I. and H. Nakagawa (1993). Turbulence in open-channel flows. *A. A. Balkema: Rotterrdam.*

Perry, A., W. Schofield and P. Joubert (1969). Rough-wall turbulent boundary layers. *Journal of Fluid Mechanics 37*, 383-413.

Seo, I. W., Y. D. Kim and C. G. Song (2014). Validation of depth-averaged flow model using flat-bottomed benchmark problems. *The scientific world journal*.

Song, T. and Y. M. Chiew (2001). Turbulence measurement in non uniform open channel flow using Acoustic Doppler Velocimeter (ADV). *Journal of Engineering Mechanics 127*, 219-232.

Soualmia, A., L. Masbernat and A. Kaffel (2010). Wall friction and momentum dispersion in free surface flows with non uniform wall roughness. *Journal of PCN 51*(1), 11-18.

Soulsby, R. L. (1980). Measurements of the Reynolds stress components close to a marine sand bank. *Marine Geology 42*, 35-47.

Stapleton, K. R. and D. A. Huntley (1995). Seabed stress determination using the inertial dissipation method and the turbulent kinetic energy method. *Earth surface processes and landforms 20*, 807-815.

Stoesser, T., R. McSherry and B. Fraga (2015). Secondary currents and turbulence over a non-uniformly roughened open channel bed. *Water 7*(9), 4896-4913.

Talbi, S. H. and A. Soualmia (2014). Momentum dispersion in free surface flows through rectangular open channels with rough beds. In *Proceedings of the 10th International Conference of Computational Methods in Sciences and Engineering,* Athens, Greece.

Townsend, A. A. (1976). The structure of turbulent shear flow. *Cambridge University Press,* New York, USA.